ATP13A2-mediated endo-lysosomal polyamine export counters mitochondrial oxidative stress

Stephanie Vrijsen[a,1], Laura Besora-Casals[b,1], Sarah van Veen[a], Jeffrey Zielich[b], Chris Van den Haute[c,d], Norin Nabil Hamouda[a], Christian Fischer[b,e], Bart Ghesquière[f], Ivailo Tournev[g], Patrizia Agostinis[h], Veerle Baekelandt[c], Jan Eggermont[a], Eric Lambie[b,i,2], Shaun Martin[a,2], and Peter Vangheluwe[a,2,3]

[a]Laboratory of Cellular Transport Systems, Department of Cellular and Molecular Medicine, Katholieke Universiteit Leuven (KU Leuven), 3000 Leuven, Belgium; [b]Cell and Developmental Biology, Department Biology II, Ludwig Maximilians Universität, 80539 Münich, Germany; [c]Laboratory for Neurobiology and Gene Therapy, Department of Neurosciences, KU Leuven, 3000 Leuven, Belgium; [d]Leuven Viral Vector Core, KU Leuven, 3000 Leuven, Belgium; [e]Center for Integrated Protein Science, Ludwig Maximilians Universtät, 80539 Münich, Germany; [f]Metabolomics Expertise Center, Vlaams Instituut voor Biotechnologie (VIB)-KU Leuven Center for Cancer Biology, Department of Oncology, KU Leuven, 3000 Leuven, Belgium; [g]Department of Neurology, Medical University-Sofia, 1431 Sofia, Bulgaria; [h]Laboratory of Cell Death Research and Therapy, VIB-KU Leuven Center for Cancer Biology, Department of Cellular and Molecular Medicine, KU Leuven, 3000 Leuven, Belgium; and [i]Department of Cell and Developmental Biology, University College London, WC1E 6BT London, United Kingdom

Edited by Stuart A. Lipton, Scripps Research Institute, La Jolla, CA, and accepted by Editorial Board Member Nancy Y. Ip October 20, 2020 (received for review December 20, 2019)

Recessive loss-of-function mutations in *ATP13A2* (*PARK9*) are associated with a spectrum of neurodegenerative disorders, including Parkinson's disease (PD). We recently revealed that the late endo-lysosomal transporter ATP13A2 pumps polyamines like spermine into the cytosol, whereas ATP13A2 dysfunction causes lysosomal polyamine accumulation and rupture. Here, we investigate how ATP13A2 provides protection against mitochondrial toxins such as rotenone, an environmental PD risk factor. Rotenone promoted mitochondrial-generated superoxide (MitoROS), which was exacerbated by ATP13A2 deficiency in SH-SY5Y cells and patient-derived fibroblasts, disturbing mitochondrial functionality and inducing toxicity and cell death. Moreover, ATP13A2 knockdown induced an ATF4-CHOP-dependent stress response following rotenone exposure. MitoROS and ATF4-CHOP were blocked by MitoTEMPO, a mitochondrial antioxidant, suggesting that the impact of ATP13A2 on MitoROS may relate to the antioxidant properties of spermine. Pharmacological inhibition of intracellular polyamine synthesis with α-difluoromethylornithine (DFMO) also increased MitoROS and ATF4 when ATP13A2 was deficient. The polyamine transport activity of ATP13A2 was required for lowering rotenone/DFMO-induced MitoROS, whereas exogenous spermine quenched rotenone-induced MitoROS via ATP13A2. Interestingly, fluorescently labeled spermine uptake in the mitochondria dropped as a consequence of ATP13A2 transport deficiency. Our cellular observations were recapitulated in vivo, in a *Caenorhabditis elegans* strain deficient in the ATP13A2 ortholog *catp-6*. These animals exhibited a basal elevated MitoROS level, mitochondrial dysfunction, and enhanced stress response regulated by *atfs-1*, the *C. elegans* ortholog of ATF4, causing hypersensitivity to rotenone, which was reversible with MitoTEMPO. Together, our study reveals a conserved cell protective pathway that counters mitochondrial oxidative stress via ATP13A2-mediated lysosomal spermine export.

neurodegeneration | antioxidant | mitochondria | P5B-type ATPase | polyamine transport

Loss-of-function mutations in *ATP13A2* (*PARK9*) are causative for a spectrum of neurodegenerative disorders, including Kufor-Rakeb syndrome (KRS, a juvenile onset parkinsonism with dementia) (1), early-onset Parkinson's disease (PD) (2, 3), hereditary spastic paraplegia (HSP) (4), neuronal ceroid lipofuscinosis (5), and amyotrophic lateral sclerosis (6), which are commonly hallmarked by lysosomal and mitochondrial dysfunction (4, 6, 7). Also, ATP13A2 deficiency causes lysosomal and mitochondrial impairment in various models, as evidenced by decreased lysosomal functionality (8, 9), reduced mitochondrial clearance capacity (8–10), mitochondrial fragmentation, mitochondrial DNA damage, and increased oxygen consumption (11, 12).

We recently discovered that ATP13A2 transports the polyamines spermidine and spermine from the late endo/lysosome to the cytosol (9). Polyamines are ubiquitous polycationic aliphatic amines that stabilize nucleic acids, influence protein folding, regulate ion channels, and modulate cell proliferation and differentiation (13–15). We found that the late endo-lysosomal transporter ATP13A2 strongly contributes to the total cellular polyamine content via a two-step process: Firstly, polyamines

Significance

Mutations in *ATP13A2* cause a spectrum of related neurodegenerative disorders. ATP13A2 is a lysosomal exporter of polyamines that contributes to lysosomal health and controls cellular polyamine content. Conversely, loss of ATP13A2 leads to lysosomal dysfunction, a hallmark of neurodegeneration. Here, we show that polyamines transported by ATP13A2 provide cellular protection by lowering reactive oxygen species (ROS), which may relate to the antioxidant properties of polyamines. Consequently, dysfunctional ATP13A2 sensitizes cells to oxidative stress, which impairs mitochondria, and induces toxicity and cell death. ATP13A2-mediated polyamine transport represents a conserved pathway that protects against mitochondrial oxidative stress. The combined protective impact of ATP13A2 on lysosomal health and mitochondrial oxidative stress may explain why ATP13A2 exerts potent neuroprotective effects.

Author contributions: E.L., S.M., and P.V. designed the study; S.V. and S.M. performed and analyzed all cell biology experiments; L.B.-C., J.Z., C.F., and E.L. conducted and analyzed *C. elegans* experiments; C.V.d.H. generated stable cell lines and analyzed ATP13A2 knockdown; B.G. performed metabolomics; N.N.H. performed mRNA analysis of ODC/AMD1; S.v.V., I.T., P.A., V.B., and J.E. provided valuable scientific input, tools and/or resources; and S.V., S.M., and P.V. wrote the paper, which was reviewed by all authors.

Competing interest statement: Patent WO-2018002350-A1 of KU Leuven describes methods for detecting compounds with therapeutic use that target ATP13A2 or related isoforms using biological material and assays described in the current manuscript. A second patent of KU Leuven describing ATP13A2 cell models described in this manuscript has also been filed.

This article is a PNAS Direct Submission. S.A.L. is a guest editor invited by the Editorial Board.

[1]S.V. and L.B.-C. contributed equally to this work.

[2]E.L., S.M., and P.V. contributed equally to this work.

[3]To whom correspondence may be addressed. Email: peter.vangheluwe@kuleuven.be.

This article contains supporting information online at https://www.pnas.org/lookup/suppl/doi:10.1073/pnas.1922342117/-/DCSupplemental.

First published November 23, 2020.

enter the cell via endocytosis and subsequently, polyamines are transported by ATP13A2 into the cytosol (9). This process complements polyamine biosynthesis via the ornithine decarboxylase (ODC) pathway (9). Importantly, ATP13A2's polyamine transport function is crucial for its neuroprotective effect, since it prevents lysosomal polyamine accumulation and subsequent lysosomal rupture, while improving lysosomal health and functionality (9). Moreover, when activated by its two regulatory lipids—phosphatidylinositol-3,5-bisphosphate [PI(3,5)P2] and phosphatidic acid (PA)—ATP13A2 exerts a cell protective effect against the mitochondrial neurotoxin rotenone (16), an environmental risk factor for PD (17). Rotenone is a mitochondrial complex I inhibitor, which leads to high levels of reactive oxygen species (ROS), promoting protein aggregation and damaging organelles. However, how ATP13A2's polyamine transport function exerts a cell protective effect against rotenone, or other mitochondrial neurotoxins, is not yet clear.

Interestingly, the transported substrates spermine and spermidine reduce oxidative stress (14, 15). Spermine is a potent free radical scavenger (18) and a biologically important antioxidant (19–23). We therefore hypothesize that ATP13A2-mediated polyamine transport may counteract oxidative stress (16, 24) and preserve mitochondrial health (11, 12). Here, we demonstrate in complementary human cell models and *Caenorhabditis elegans* that lysosomal polyamine export by ATP13A2 effectively lowers ROS levels and promotes mitochondrial health and functionality, pointing to a lysosomal-dependent cell protective pathway that may be implicated in ATP13A2-related neurodegenerative disorders.

Results

ATP13A2 Protects Cells and Mitochondria against Mitochondrial Toxins. We previously validated stable human neuroblastoma (SH-SY5Y) cell models with either ATP13A2 knockdown (sh-ATP13A2/kd) or wild-type ATP13A2 overexpression (WT-OE), and control cell lines with overexpression or shRNA-mediated knockdown of firefly luciferase (Fluc or sh-Fluc, respectively) (16). ATP13A2 expression offered protection, whereas knockdown exacerbated toxicity against rotenone (17) (Fig. 1*A* and *SI Appendix*, Fig. S1 *A* and *B*), but also against other mitochondrial neurotoxins such as 1-methyl-4-phenylpyridinium (MPP^+) and 6-hydroxydopamine hydrobromide (6-OHDA) (25, 26) (*SI Appendix*, Fig. S1 *C–F*). The increased rotenone toxicity in kd cells was associated with a drop in mitochondrial membrane potential (MMP) (Fig. 1*B*) and ATP production (Fig. 1*C*), whereas ATP13A2 overexpression prevented the reduction in MMP (Fig. 1*B*). Interestingly, fibroblasts isolated from patients with HSP and KRS that harbor homozygous loss-of-function mutations in ATP13A2 (T512I and F851CfsX856, respectively) (4, 12, 27) also present a higher rotenone sensitivity, which is reflected by increased cell death (Fig. 1*D*) and a rotenone-induced decrease in MMP (Fig. 1*E*). Thus, ATP13A2 reduces toxicity and mitochondrial dysfunction induced by mitochondrial toxins.

Loss of ATP13A2 Increases Mitochondrial ROS, Which Activates an ATF4-Dependent Stress Response. Since ATP13A2's transported substrates spermine and spermidine are potent antioxidants (14, 15), and rotenone causes ROS accumulation (28), we examined the impact of ATP13A2 on ROS levels. Using the probes 2′,7′-dichlorofluorescin diacetate (DCFDA) (29) and MitoSOX (30) in the SH-SY5Y cell models, we showed that rotenone, MPP^+, and 6-OHDA increased the production of a broad range of ROS (*SI Appendix*, Fig. S2*A*) and superoxide (i.e., ROS originating from mitochondria, hence referred to as MitoROS) (30) (*SI Appendix*, Fig. S2*B*), respectively. As early as 2 h posttreatment, ATP13A2 kd cells exhibited significantly higher MitoROS accumulation upon rotenone exposure, which was lower in WT-OE cells (*SI Appendix*, Fig. S3). While the antioxidant *N*-acetylcysteine (NAC) reduced rotenone-induced ROS (Fig. 2*A*) and MitoROS (Fig. 2*B*) levels, the mitochondrial targeted antioxidant MitoTEMPO, which quenches superoxides, completely abolished rotenone-induced MitoROS accumulation (Fig. 2*C*). Moreover, MitoTEMPO lowered MitoROS in the ATP13A2 kd and Fluc cells to a similar level as observed in WT-OE cells (Fig. 2*C*), indicating that ATP13A2 provided a comparable antioxidant effect as MitoTEMPO. In patient-derived fibroblasts, MitoTEMPO counteracted the higher MitoROS to comparable levels as in wild-type fibroblasts (Fig. 2*D*). In both cell models, the decrease in MitoROS by MitoTEMPO was accompanied by a diminished cell death in rotenone conditions (*SI Appendix*, Fig. S4).

It has been reported that MitoROS accumulation leads to increased ATF4 expression, a transcription factor that activates an antioxidant response and promotes mitochondrial homeostasis (31). Also, ATP13A2 kd cells presented a strong up-regulation of ATF4, peaking at 6 h when challenged with rotenone (Fig. 3*A*), serving as an independent confirmation of the increased MitoROS levels. In addition, ATF4 up-regulated the proapoptotic transcription factor CHOP, which was elevated after 12 to 24 h in ATP13A2 kd cells (Fig. 3*B*). After 24 h, we further noted an up-regulation of the mitochondrial chaperone HSP60 (Fig. 3*C*), which most likely falls under control of CHOP (32). Interestingly, MitoTEMPO treatment prevented the rotenone-induced up-regulation of both ATF4 and CHOP expression in ATP13A2 kd cells (Fig. 3*D*), indicating that the increased MitoROS in ATP13A2 kd cells underlies the ATF4-driven stress response. No effect was observed on ATF5 and C/EBPβ expression, highlighting the specificity of the ATF4 stress response as a consequence of MitoROS accumulation (*SI Appendix*, Fig. S5).

The mitochondrial phenotype and stress response observed in ATP13A2 kd cells are most likely caused by the induction of MitoROS, rather than as a consequence of cell death. Indeed, kd cells already presented a clear increase in MitoROS (*SI Appendix*, Fig. S3) and initiation of the MitoROS-dependent stress response (Fig. 3*A*) as early as 6 h post rotenone exposure, resulting in a decreased MMP, even though cell death was not yet significantly increased (*SI Appendix*, Fig. S6).

Taken together, ATP13A2 reduces MitoROS accumulation in rotenone conditions preventing the activation of a MitoROS-induced stress pathway and cell death initiation.

Spermine Transported by ATP13A2 Reduces MitoROS. Next, we tested whether the impact of ATP13A2 on MitoROS depends on the polyamine transport function of ATP13A2, rather than on its transport-independent scaffold function (33). Indeed, WT-OE strongly reduced MitoROS in the presence of rotenone, whereas expression of a transport-inactive ATP13A2 mutant (D508N-OE) (9) had no effect (Fig. 4*A*), despite comparable expression of D508N-OE and WT-OE (16). Moreover, pharmacological inhibition of the formation of the regulatory lipids PI(3,5)P2 and PA, which activate ATP13A2 transport (9, 16, 24), abolished the impact of ATP13A2 on ROS and MitoROS (*SI Appendix*, Fig. S7), further demonstrating that the transport function of ATP13A2 is required for reducing the MitoROS levels.

We previously reported that ATP13A2 activity critically contributes to the native polyamine content as well as the cellular uptake of BODIPY-labeled polyamines spermidine and spermine (9, 34), reflecting the biochemical activity of ATP13A2 (9). This explains why Fluc cells exhibited higher cellular uptake of the BODIPY-spermine and -spermidine as compared to ATP13A2 kd (*SI Appendix*, Fig. S8). Interestingly, extracellular administration of a physiological concentration of 1 μM unlabeled spermine (35) fully abolished the rotenone-induced MitoROS increase in Fluc cells to similar levels as observed in WT-OE cells that are maximally protected (Fig. 4*B*), but had no significant impact on ATP13A2 kd cells (Fig. 4*B*). Together, ATP13A2 promotes uptake of extracellular spermine to counter the accumulation of MitoROS.

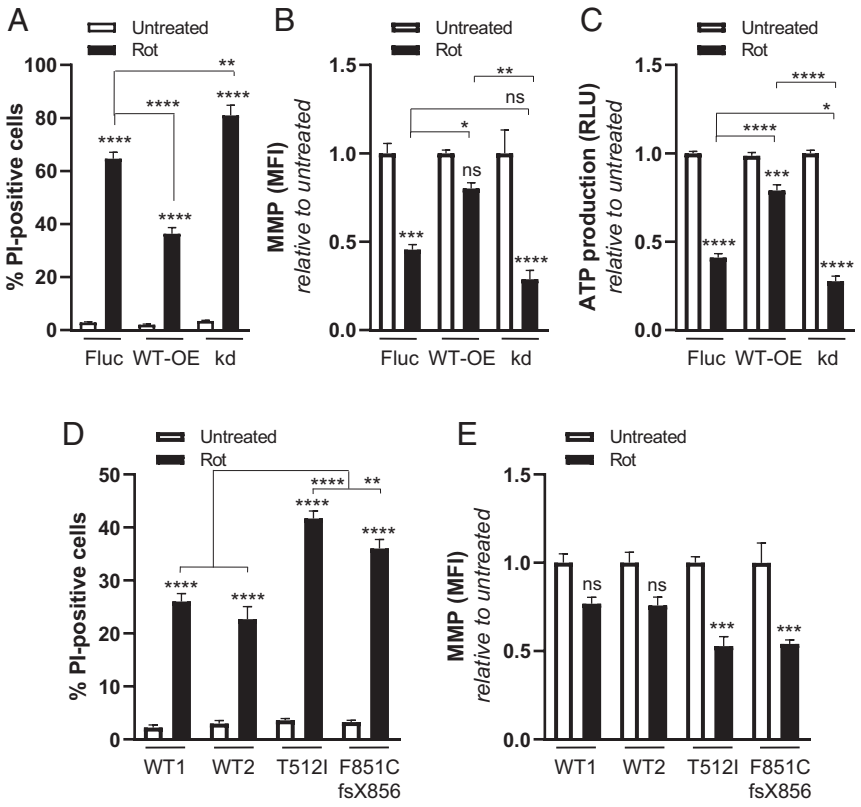

Fig. 1. ATP13A2 prevents rotenone-induced cell death and mitochondrial damage. (*A*–*C*) SH-SY5Y cells stably overexpressing firefly luciferase (Fluc, control), ATP13A2 (WT-OE), or sh-ATP13A2 (kd) and (*D* and *E*) patient-derived fibroblasts with loss-of-function mutations T512I or F851CfsX856 in ATP13A2 versus wild-type fibroblasts (WT1 and WT2) were treated with rotenone (Rot, 1 μM, 24 h). Subsequently, cell death was measured by means of a propidium iodide (PI) assay (*A* and *D*). MMP (*B* and *E*) and ATP production (*C*) were assessed as parameters of mitochondrial functionality. Data are the mean of a minimum of three independent experiments ± SEM. RLU, relative luminescence units; MFI, mean fluorescence intensity. $*P < 0.05$; $**P < 0.01$; $***P < 0.001$; $****P < 0.0001$; ns, nonsignificant versus respective untreated unless depicted otherwise; ANOVA post hoc Tukey's multiple comparison test.

Inhibition of Polyamine Synthesis in ATP13A2-Deficient Cells Causes a MitoROS Response. Since impaired polyamine transport induced a MitoROS response, inhibition of polyamine synthesis may also elevate MitoROS in ATP13A2 kd cells. Indeed, treating ATP13A2 kd cells with α-difluoromethylornithine (DFMO), a compound that blocks ODC (a rate-limiting enzyme of polyamine synthesis), resulted in higher MitoROS levels (Fig. 4*C*) and ATF4-CHOP upregulation (Fig. 4*D*), which was accompanied by a significant increase in cell death (Fig. 4*E*). As expected from the reduced ATP13A2 activity, this could not be prevented by exogenous spermine, whereas MitoTEMPO completely prevented the initiation of a stress response and cell death in ATP13A2 kd cells subjected to DFMO (Fig. 4 *D* and *E*). In Fluc cells, DFMO resulted in a nonsignificant increase of MitoROS that was completely prevented by exogenous spermine addition, whereas no MitoROS accumulation was observed in WT-OE cells (Fig. 4*C*). Thus, DFMO treatment mimics the rotenone phenotype in ATP13A2 kd cells, pointing to a direct effect of the transported polyamines on MitoROS, the stress response, and cell death.

Importantly, we independently recapitulated both the rotenone and DFMO phenotypes (*SI Appendix*, Fig. S9) in CRISPR/Cas9-mediated ATP13A2 knockout cells (KO) that were recovered with either wild-type ATP13A2 (KO/WT) or the transport dead D508N mutant (KO/D508N) (9). The ATP13A2 transport deficiency in KO/D508N cells caused an increased MitoROS and ATF4-stress response in rotenone or DFMO conditions that was only rescued by MitoTEMPO, but not spermine administration (*SI Appendix*, Fig. S9 *B*–*D*).

Thus, ATP13A2-mediated spermine transport protects mitochondria by countering mitochondrial oxidative stress and complements ODC-dependent polyamine synthesis.

ATP13A2 Promotes Cellular and Mitochondrial Polyamine Uptake. Next, we examined whether the documented lysosomal dysfunction (8–10) may be responsible for the MitoROS phenotype in ATP13A2-deficient cells. While lysosomal dysfunction in ATP13A2 KO and KO/D508N cells can be restored by administration of acidic nanoparticles that enter the cells via endocytosis (9, 36), these nanoparticles had no impact on MitoROS (Fig. 5*A*), indicating that lysosomal dysfunction is not the underlying cause of the MitoROS phenotype. Instead, MitoROS levels may be a direct consequence of a reduced polyamine content, which we examined here via metabolomics. As observed before (9), the native polyamine levels in KO/D508N cells versus KO/WT were significantly decreased in untreated conditions (*SI Appendix*, Fig. S9*E*), however, without evoking a significant MitoROS response (*SI Appendix*, Fig. S9*B*). Putrescine and spermidine levels were further reduced in KO/D508N cells exposed to DFMO (Fig. 5*B*), in line with higher MitoROS (*SI Appendix*, Fig. S9*B*). DFMO had no significant effect on spermine levels (Fig. 5*B*), as observed before (37). In KO/WT cells, the combined polyamine pool (*SI Appendix*, Fig. S9*E*), and also MitoROS levels (*SI Appendix*, Fig. S9*B*), were not significantly affected by DFMO, indicating that ATP13A2-mediated polyamine uptake activity adequately compensated for the inhibition of polyamine synthesis in these cells, possibly due to the relatively higher ATP13A2 expression in KO/WT versus control cells (9). Moreover, adding exogenous spermine in DFMO conditions

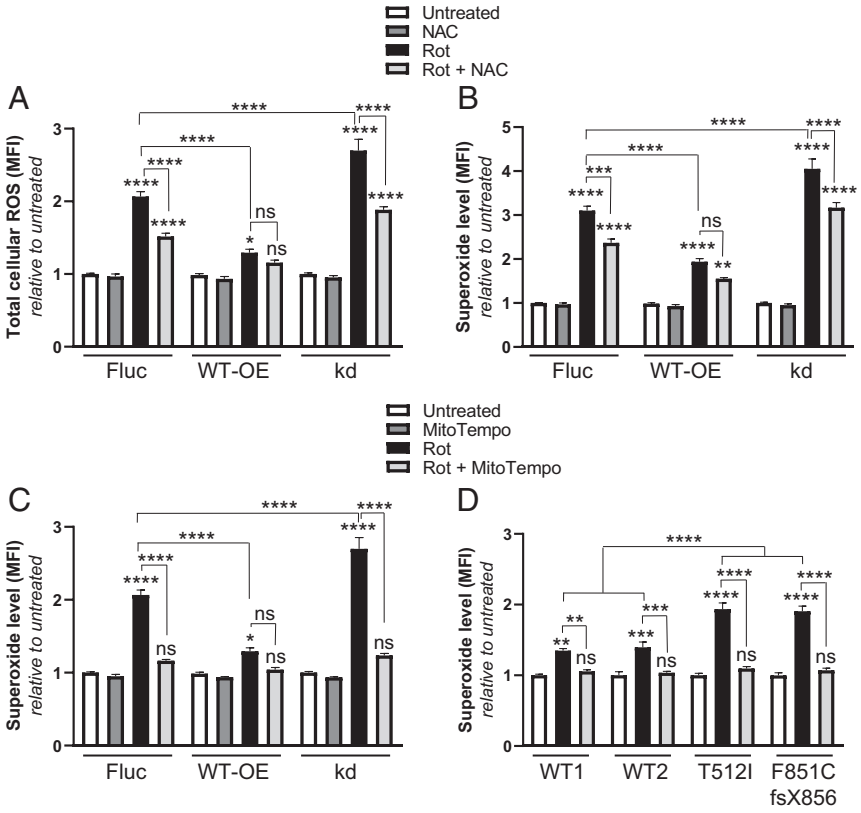

Fig. 2. ATP13A2 prevents the accumulation of mitochondrial-generated ROS. (*A*–*C*) In SH-SY5Y cells stably overexpressing Fluc (control), ATP13A2 (WT-OE), or sh-ATP13A2 (kd), total cellular ROS (*A*) or mitochondrial-generated superoxide (*B* and *C*) levels were analyzed by means of DCFDA or MitoSOX probes, respectively, followed by flow cytometry. Cells were pretreated (1 h) or not with a general (NAC, 2 mM; *A* and *B*) or a mitochondrial-specific superoxide scavenger (MitoTEMPO, 1 μM; *C*) before adding rotenone (Rot, 1 μM, 24 h). In human patient-derived fibroblasts (*D*), the same experimental setup was used (Rot, 1 μM, 24 h), and pretreatment with MitoTEMPO (1 μM) decreased the MitoROS levels induced by Rot to levels similar to those seen in WT cells (WT1, WT2). Data are the mean of a minimum of three independent experiments ± SEM. MFI, mean fluorescence intensity. *$P < 0.05$; **$P < 0.01$; ***$P < 0.001$; ****$P < 0.0001$; ns, nonsignificant versus respective untreated unless depicted otherwise; ANOVA post hoc Tukey's multiple comparison test.

led to a significantly higher polyamine content in DFMO-treated KO/WT cells (*SI Appendix*, Fig. S9*E*), but not in KO/D508N cells, indicating again that KO/WT cells can maintain their polyamine levels by taking up spermine, in contrast to KO/D508N cells.

To further examine spermine uptake and subcellular distribution, we turned to confocal microscopy to detect BODIPY-labeled spermine in ATP13A2 KO cell models. ATP13A2 promoted BODIPY-spermine transport to the mitochondria, as evidenced by the significantly higher basal colocalization between BODIPY-spermine and the mitochondrial marker TOMM22 in KO/WT cells versus KO/D508N cells (Fig. 5*C*). Moreover, the mean fluorescent intensity of BODIPY-spermine within the mitochondrial network was significantly higher in KO/WT cells (Fig. 5*D*).

Thus, spermine transported by ATP13A2 is redistributed to the mitochondria, where it may locally counteract MitoROS accumulation and protect mitochondrial function irrespective of lysosomal deficiency.

The MitoROS Protective Response via ATP13A2 Is Highly Conserved and Relevant In Vivo. Finally, we validated whether the antioxidant effect of ATP13A2 and the subsequent prevention of a stress response are conserved among species and may be relevant in vivo. Therefore, we turned to a *C. elegans* strain that is defective in *catp-6*, one of three related nematode orthologs that has the largest similarity with ATP13A2 because of its late endo-lysosomal localization (38, 39). The *C. elegans catp-6(ok3473)* animals were hypersensitive to rotenone (Fig. 6*A*). Moreover, a reduced MMP was already evident under basal conditions in the *catp-6(ok3473)* strain, which was further aggravated in the presence of rotenone (Fig. 6*B* and *SI Appendix*, Fig. S10*A*) and partially rescued by MitoTEMPO (Fig. 6*C* and *SI Appendix*, Fig. S10*B*). Moreover, MitoROS levels were constitutively elevated in *catp-6(ok3473)* animals, and further increased by rotenone exposure (Fig. 6*D* and *SI Appendix*, Fig. S10*C*). MitoTEMPO diminished MitoROS accumulation (Fig. 6*D* and *SI Appendix*, Fig. S10*C*) and lethality (Fig. 6*E*) in response to rotenone. The reexpression of wild-type *catp-6* rescued the MitoROS phenotype, while the catalytically inactive mutant *catp-6(D465N)* did not, demonstrating the requirement of transport activity (Fig. 6*D*). With a P*hsp-60::GFP* reporter, a marker for *hsp-60* expression (40), we observed that *catp-6* mutant worms presented a constitutively induced mitochondrial stress response (Fig. 6*F* and *SI Appendix*, Fig. S10*D*). This response could be partially rescued by reexpression of wild-type *catp-6* (Fig. 6*F* and *SI Appendix*, Fig. S10*D*) or by the addition of MitoTEMPO (Fig. 6*G* and *SI Appendix*, Fig. S10*D*). Knockdown of *atfs-1*, the closest ortholog to mammalian ATF4, down-regulated the expression of the P*hsp-60::GFP* reporter (Fig. 6*H* and *SI Appendix*, Fig. S10*D*), indicating that *atfs-1* is at least partially responsible for the *hsp-60* up-regulation in the *catp-6(ok3473)* animals. Of the three *C. elegans* orthologs, *catp-6* appears the most relevant isoform that phenocopies mammalian ATP13A2 (39), since the triple *catp-7(0) catp-6(0); catp-5(0)* null mutant displayed a similar MMP phenotype to the *catp-6(ok3473)* animals (*SI Appendix*, Fig. S10*E*).

In conclusion, like ATP13A2 in human cells, *catp-6* counters mitochondrial oxidative stress in *C. elegans*, which prevents the up-regulation of an ATF4/*atfs-1*-dependent response.

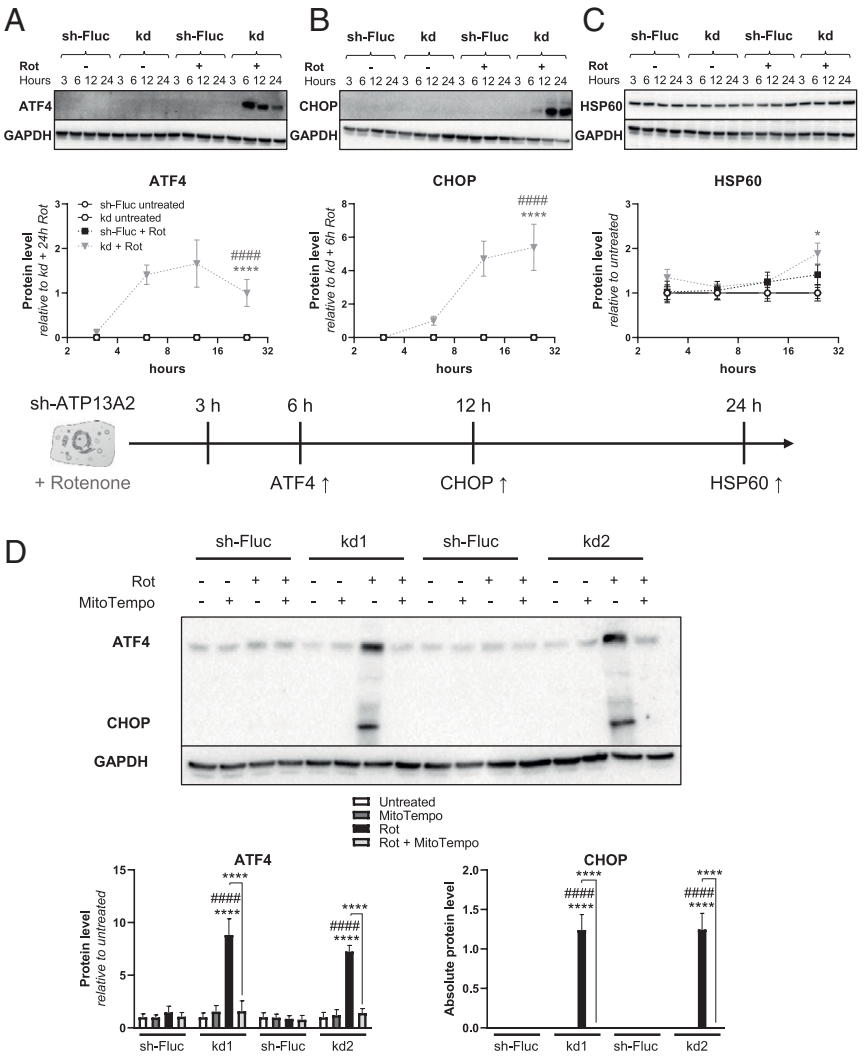

Fig. 3. ATP13A2's antioxidative effect prevents an ATF4-dependent stress response. SH-SY5Y cells stably overexpressing sh-Fluc (control) or sh-ATP13A2 (kd) were (*A*–*C*) treated with rotenone (Rot, 1 μM), and protein levels of various cellular stress markers were followed over a time span of 24 h. Immunoblotting was performed for the transcription factors (*A*) ATF4 and (*B*) CHOP, and for (*C*) the mitochondrial chaperone HSP60. All obtained protein levels were normalized for GAPDH before plotting relative to the condition indicated in the bar graph axis. (*D*) Rot (1 μM, 24 h) treatment combined with the mitochondrial superoxide scavenger MitoTEMPO (1 μM, 1 h pretreatment + 24 h) prevented the up-regulation of the stress response proteins ATF4 and CHOP (kd1 and kd2 indicate that two different knockdown cell lines were used, stably transduced with two different shRNAs targeting ATP13A2). Data are the mean of a minimum of three independent experiments ± SEM. $^{*}P < 0.05$, $^{**}P < 0.01$, $^{***}P < 0.001$, $^{****}P < 0.0001$ versus respective untreated unless depicted otherwise; $^{\#\#\#\#}P < 0.0001$ versus rotenone-treated sh-Fluc; ANOVA post hoc Tukey's multiple comparison test.

Discussion

Lysosomal Spermine Export via ATP13A2 Promotes Lysosomal and Mitochondrial Health. Our current study offers compelling insights into the physiological role of ATP13A2 as a polyamine transporter placed at the intersection of lysosomes and mitochondria. We previously reported that ATP13A2 maintains healthy and functional lysosomes by preventing toxic lysosomal accumulation of polyamines (9). In addition, a reduced ATP13A2 activity lowers the cellular polyamine content and impairs cellular polyamine distribution (9). Here, we showed that this contributes to downstream problems. Our findings show that ATP13A2-mediated lysosomal polyamine export lowers mitochondrial-derived ROS and improves mitochondrial function (*SI Appendix*, Fig. S11). The dual impact of ATP13A2-mediated polyamine transport on lysosomal and mitochondrial health may explain why ATP13A2 exerts a strong neuroprotective effect and why ATP13A2 deficiency is associated with neurological disorders hallmarked by lysosomal and mitochondrial dysfunction (41).

Lysosomal Spermine Export Exerts an Antioxidant Response That Protects Mitochondria. The phenotypes we observe in our ATP13A2/*catp-6*-deficient models are clearly MitoROS driven. The increased lethality, high (Mito)ROS levels, aberrant MMP, and stress response induction can all be reversed by the MitoROS scavenger MitoTEMPO or a functional ATP13A2/*catp-6*, but not by a transport inactive mutant. We showed that polyamines provide the basis of the protective effect toward mitochondrial complex I inhibition and subsequent MitoROS accumulation. The impact of ATP13A2's transport function on MitoROS can be explained by the antioxidant properties of spermine and spermidine, which are potent free radical scavengers (14, 15, 18–23).

Here, we report the redistribution of extracellular spermine to mitochondria, which is facilitated via ATP13A2-mediated endo-lysosomal export, but the nature of the mitochondrial polyamine transporter remains unknown. There are multiple reports describing the uptake of polyamines into mitochondria (42–44), which regulate MMP (45), oxidative phosphorylation (45), and enzymes of the Krebs cycle (46–48), and/or act as free radical

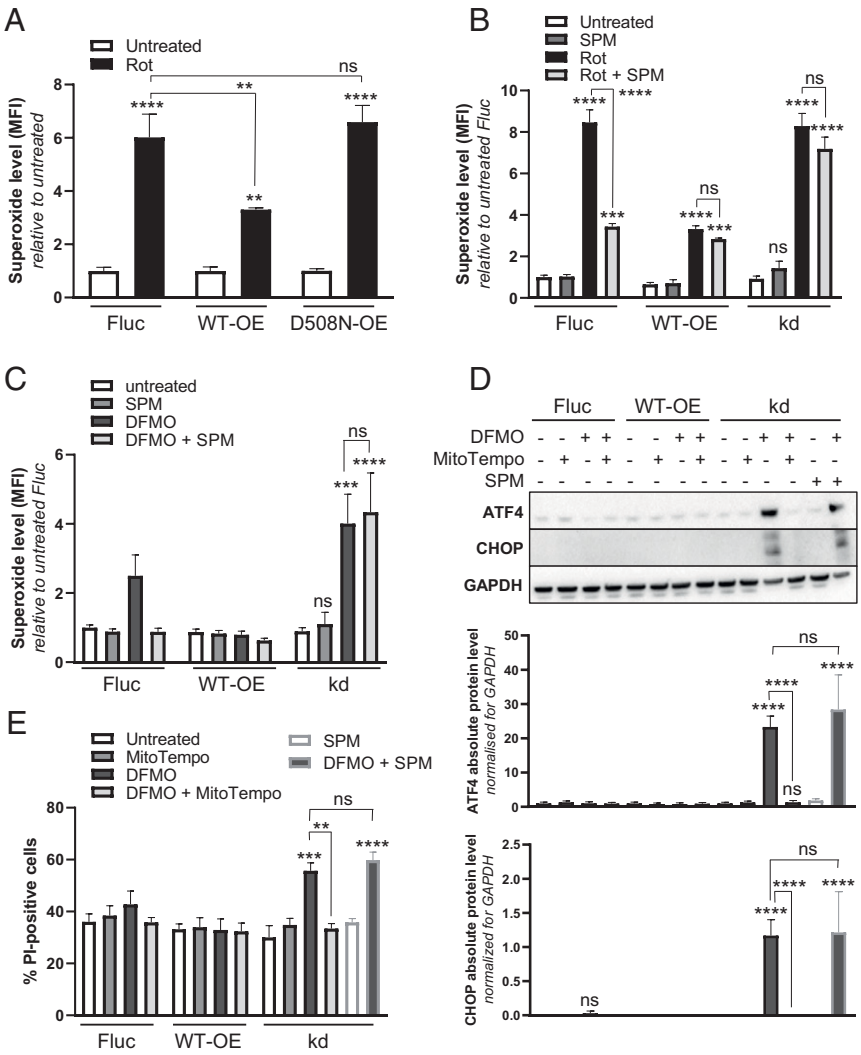

Fig. 4. Spermine transported by ATP13A2 provides protection toward oxidative stress, thereby preventing the activation of a stress response. SH-SY5Y cells stably overexpressing Fluc (control), ATP13A2 (WT-OE), catalytically inactive D508N ATP13A2 (D508N-OE), or sh-ATP13A2 (kd) were treated with rotenone (Rot, 1 μM, 24 h; *A* and *B*) or DFMO (0.1 mM, 48 h; *C*–*E*) with or without spermine (SPM) (1 μM; *B*–*E*; last 24 h) or MitoTEMPO (1 μM; *D* and *E*; last 24 h). Subsequently, superoxide levels were measured with the MitoSOX probe (*A*–*C*), protein levels of stress response markers ATF4 and CHOP were assessed via immunoblotting (*D*), or cell death readout was performed by means of a propidium iodide assay with flow cytometry (*E*). Data are the mean of a minimum of three independent experiments ± SEM. MFI, mean fluorescence intensity. $^{**}P < 0.01$; $^{***}P < 0.001$; $^{****}P < 0.0001$; ns, nonsignificant versus respective untreated unless depicted otherwise, ANOVA post hoc Tukey's multiple comparison test.

scavenger inside mitochondria (49). ATP13A2 potently reduces MitoROS, indicating that polyamines may quench superoxide in or near the mitochondria (49). ATP13A2-mediated polyamine transport may also regulate MMP, as evidenced by the higher MMP in our WT-OE cells, or mitophagy, explaining the higher mitochondrial volume consistently reported in cells with ATP13A2 deficiency (11, 12). Additional studies are under way to further dissect the role of ATP13A2 in mitochondrial–lysosomal cross-talk, interactions, and polyamine transfer.

Synergy between ATP13A2-Mediated Polyamine Transport and Polyamine Metabolism. A dynamic interplay between polyamine uptake and metabolism has been repeatedly reported, but the relative contribution of polyamine uptake versus synthesis may be cell-type dependent. Various cell models present different DFMO sensitivities, and our observations indicate that ATP13A2 activity modulates DFMO sensitivity (9). We found that ATP13A2 plays a prominent role in controlling the cellular polyamine content and synergizes with the ODC pathway for polyamine synthesis. Indeed, deletion of ODC and ATP13A2 orthologs are synthetically lethal in *Saccharomyces cerevisiae* (50) and *C. elegans* (51). Also, ATP13A2 KO and KO/D508N cells display a strong reduction in polyamine levels, indicating that ODC activity is unable to compensate for the loss of polyamine uptake, despite an up-regulation of ODC mRNA expression (*SI Appendix*, Fig. S9*F*). DFMO treatment elevates ROS levels and triggers an ATF4-dependent stress response specifically in ATP13A2-deficient cells. Based on these observations, we speculate that consequences of ATP13A2 dysfunction may be strongest in cell types that are more reliant on polyamine uptake than on polyamine synthesis to maintain the endogenous polyamine pool. DFMO treatment caused a reduction in putrescine and spermidine in KO/D508N cells, but not spermine, as reported before (37), whereas spermine administration affected putrescine and spermidine levels, but not spermine content, indicating that the spermine pool is most strictly regulated. Due to polyamine interconversions and redistribution, it remains difficult to correlate changes in MitoROS levels to local changes in specific polyamine types. Future studies will be needed to determine the contribution of other enzymes in

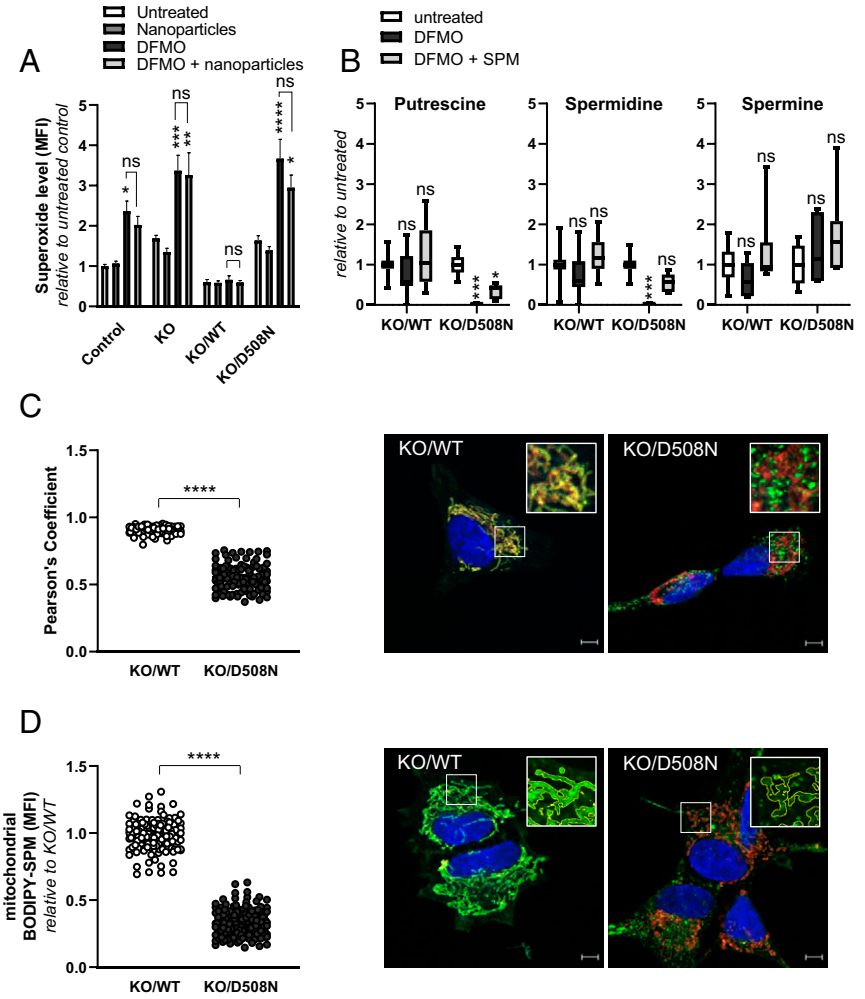

Fig. 5. Spermine transported by ATP13A2 is redistributed to the mitochondria. SH-SY5Y neuroblastoma cells with endogenous ATP13A2 levels (control) or with ATP13A2 KO overexpressing WT ATP13A2 (KO/WT), or a catalytically dead mutant ATP13A2 (KO/D508N) were exposed to DFMO (1 mM, 48 h; *A* and *B*), nanoparticles (180 ng/mL, 1 h incubation before DFMO addition) (*A*), spermine (SPM, 1 μM, 6 h; *B*), BODIPY-labeled spermine (BODIPY-SPM, 1 μM, 90 min; *C* and *D*), or a combination thereof. Subsequently, superoxide levels were assessed with the MitoSOX probe (*A*), polyamine levels were determined via metabolomics of total cell lysates (*B*), or cells were fixed and stained for TOMM22 to analyze colocalization (yellow) of BODIPY-SPM (green) and TOMM22 (red) (*C*) or BODIPY-SPM mean fluorescence intensity within the TOMM22-stained mitochondrial network (*D*, yellow borders represent mitochondria). Representative images are shown, boxed areas are enlarged in the *Inset*. For the analysis in *C*, images were taken with settings optimized for the individual cell lines. For the analysis in *D*, images were taken with equal settings to enable a comparison of mitochondrial BODIPY-SPM mean fluorescence intensity between the cell lines (Scale bar, 5 μm.) Data are the mean of a minimum of three independent experiments ± SEM. In each experiment, data are gathered of two isogenic cell lines (for control, KO, KO/WT, and KO/D508N) of which the average is displayed. MFI, mean fluorescence intensity. $*P < 0.05$, $**P < 0.01$, $***P < 0.001$, $****P < 0.0001$; ns, nonsignificant versus respective untreated (*A* and *B*), or KO/WT (*C* and *D*) unless depicted otherwise, ANOVA post hoc Tukey's or Dunnett's multiple comparison test (*A* and *B*, respectively), Mann–Whitney *U* test (*C*), or two-tailed unpaired *t* test (*D*).

polyamine metabolism, while following the subcellular polyamine content, interconversions, and distribution.

ATP13A2 and Polyamines Are Implicated in Oxidative Stress Responses. ATP13A2 and its transported substrates have been reported before to protect against conditions of oxidative stress and oxidative stress pathways (52–54). ATP13A2's potent antioxidant effect may be key to confer mitochondrial protection to various ROS-inducing neurotoxins such as rotenone, 6-OHDA, and MPP^+. Conversely, ATP13A2 activity promotes paraquat toxicity, which as a polyamine homolog may be taken up in cells more efficiently, possibly explaining the increased toxicity (55). Excess ROS is a main contributor of neuronal cell death, which is related to the high susceptibility of neurons to oxidative damage (56, 57). Oxidative stress in neurodegenerative disorders may arise due to a combination of mitochondrial complex I dysfunction, iron accumulation, lysosomal rupture, reduced glutathione deficiency, and impaired polyamine availability (9, 56). Interestingly, both ATP13A2 (58, 59) and spermidine supplementation (60) have been reported to diminish α-synuclein toxicity, which may at least partially relate to the antioxidant role of ATP13A2-mediated polyamine transport. Also toxic levels of heavy metals induce oxidative stress and cause ROS accumulation (61), which may explain why ATP13A2's transport activity counteracts heavy metal toxicity (16, 24, 59, 62, 63). Furthermore, hypoxia stimulates ATP13A2 transcription via HIF1α (54), which has been suggested to improve dopaminergic neuron survival (53).

MitoROS accumulation in ATP13A2-deficient cells also drives an ATF4/CHOP/HSP60-dependent stress response (32), a modulator of mitochondrial quality control (64–66). ATF4 has a major role as cell fate decision maker (67), so the ATF4-CHOP axis may exert a proapoptotic (68, 69) or prosurvival (70, 71) role in our models, which remains to be investigated.

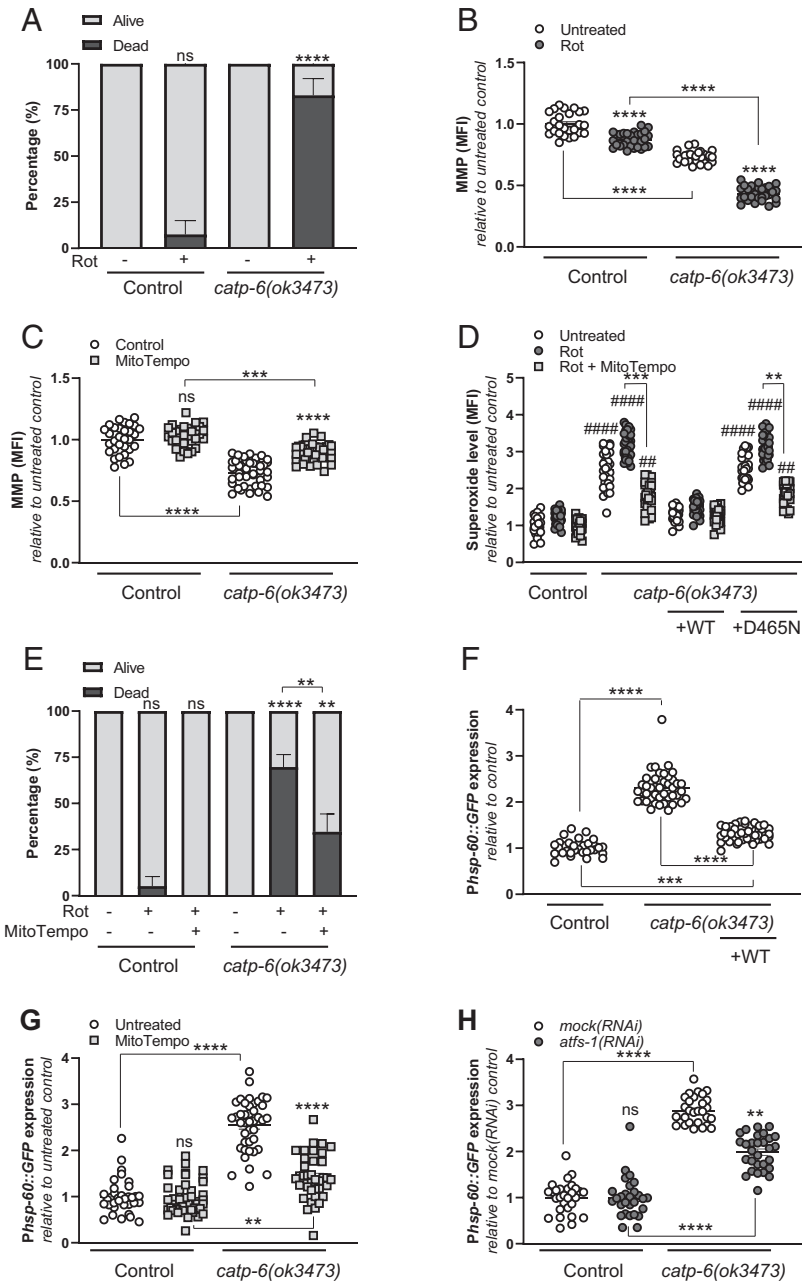

Fig. 6. The ATP13A2 ortholog *catp-6* exerts a mitochondrial protective antioxidant function in vivo in *C. elegans*, thereby preventing the activation of a stress response. WT (control) *C. elegans* and strains carrying a loss-of-function mutation (*ok3473*) in the P5B-ortholog *catp-6*, either rescued or not by overexpression of wild-type *catp-6* (WT) or a catalytically inactive mutant (D465N), were exposed to rotenone (Rot, 10 μM) (*A*, *B*, *D*, and *E*) or analyzed under basal conditions (*C*, *F*, *G*, and *H*) in absence (*A*, *B*, *F*, and *H*) or presence (*C*, *D*, *E*, and *G*) of MitoTEMPO (10 mM). Subsequently, we measured (*A* and *E*) lethality (60 h and 72 h Rot exposure, respectively), (*B* and *C*) MMP (16 h Rot exposure), (*D*) superoxide levels (16 h Rot exposure), or (*F*–*H*) expression level of the P*hsp60::GFP* reporter. In *H*, animals were treated either with *mock(RNAi)* or with *atfs-1(RNAi)*. For representative pictures of each panel, please see *SI Appendix*, Fig. S10. Data are the mean of a minimum of three independent experiments ± SEM. MFI, mean fluorescence intensity. $^{**}P < 0.01$, $^{***}P < 0.001$, $^{****}P < 0.0001$; ns, nonsignificant versus respective untreated unless otherwise indicated; $^{\#\#}P < 0.01$, $^{\#\#\#\#}P < 0.0001$ versus rotenone-treated control; ANOVA or Kruskal–Wallis with post hoc Tukey's (*A*, *B*, and *E*) or Dunn's (*C*, *D*, *F*, *G*, and *H*) multiple comparison test, respectively.

In conclusion, ATP13A2-mediated polyamine export from the late endo/lysosome into the cytosol reduces ROS generated by mitochondria, protecting mitochondrial health and preventing cell death. This highly conserved pathway counters mitochondrial oxidative stress and may contribute to ATP13A2's neuroprotective effect.

Materials and Methods

A more detailed description of the materials and methods can be found in *SI Appendix, Supplementary Materials and Methods*.

Cell Culture Conditions. SH-SY5Y neuroblastoma cell lines stably overexpressing firefly luciferase or sh-firefly luciferase (Fluc or sh-Fluc, depending on comparison with either overexpression or knockdown cell lines, respectively), *Homo sapiens* wild-type ATP13A2 (WT-OE), catalytically deficient ATP13A2 (D508N-OE) or sh-ATP13A2 (kd) were generated via lentiviral transduction as described previously (16). We made use of two independent polyclonal lines with ATP13A2 knockdown (kd1 and kd2, since two different shRNAs targeting ATP13A2 were used), of which the mean is reported in the results. Immunoblots show the independent clonal cell lines. KO of ATP13A2 and subsequent lentiviral transduction with WT (KO/WT) or D508N mutated

(KO/D508N) ATP13A2 was achieved as described previously (9). Two independent isogenic cell lines were tested, of which either the average is depicted, or in the case of immunoblots they were loaded separately. Both fibroblasts and SH-SY5Y cells were maintained at 37 °C in presence of 5% CO_2. SH-SY5Y cells were incubated in Dulbecco's Modified Eagle Medium high-glucose culture medium supplemented with 1% glutamax (Life Technology), 1% penicillin/streptomycin (Sigma), 15% fetal calf serum (heat inactivated) (Sigma), 1% nonessential amino acids (Sigma), 1% sodium pyruvate (Gibco), 10 μg/mL gentamicin (Gibco), and selection antibiotic (5 μg/mL blasticidin or 2 μg/mL puromycin [Invivogen]). All treatments were performed in the same medium, but without selection antibiotic and with 5% fetal calf serum instead of 15%. Fibroblasts were maintained in Basal Medium Eagle media (Sigma), supplemented with 100 U/mL penicillin and 100 μg/mL streptomycin. Spermine was administered in heat-inactivated fetal calf serum to inactivate serum polyamine oxidase activity.

Determination of Intracellular ATP Level. The cells were treated as indicated. Intracellular ATP was determined after saponin-based lysis of phosphate buffered saline (PBS)-washed cells. An ATP Bioluminescent assay kit (FLAAM-1VL, Sigma) was used based on luciferin-luciferase conversion, following manufacturer's instructions. Bioluminescence was assessed by optical top reading via a Flex Station 3 microplate reader (Molecular Devices Inc.).

SDS/PAGE and Immunoblotting. Cells were seeded at 3×10^6 or 2×10^6 cells/10-cm dish, depending on whether the subsequent treatment would take 24 or 48 h, respectively. After treatment for the indicated time periods, cells were harvested and subsequently lysed with radio-immunoprecipitation assay buffer (89900, Thermo Fisher Scientific) supplemented with protease inhibitors (S8820, Sigma). Next, protein concentration was determined by means of a bicinchoninic acid protein assay. SDS/PAGE (sodium dodecyl-sulfate polyacrylamide gel electrophoresis) and immunoblotting were performed as described in (24).

Analysis of BODIPY-spermine Uptake and Redistribution via Immunocytochemistry. Cells were seeded at 50,000 cells/well in a 12-well plate with coverslips. Next day, cells were treated with 1 μM BODIPY-labeled spermine for 90 min at 37 °C. Afterward, cells were processed for immunocytochemistry as described in ref. 9. Samples were then mounted and images were acquired using an LSM780 confocal microscope (Zeiss) with a 63× objective. For the colocalization analysis (Fig. 5*C*), images were taken with settings optimized for the individual cell lines. Both for KO/WT and KO/D508N, >75 images were used for analysis. To analyze BODIPY-spermine mean fluorescence intensity within the mitochondrial network (Fig. 5*D*), images were taken with equal settings to enable a comparison of mitochondrial BODIPY-spermine intensity between the cell lines. Both for KO/WT and KO/D508N, >145 individual cells were used for analysis.

Cell Viability Assay. Cell viability was assessed by means of a 4-methylumbelliferyl heptanoate (MUH, M2514, Sigma) assay. Cells seeded at a density of 10,000 cells/well in a 96-well plate were washed with PBS (without Ca^{2+} and Mg^{2+}) (Sigma) followed by incubation with 0.01 mg/mL MUH (30 min, 37 °C). End-point measurement was assessed with a Flex Station plate reader (Molecular Devices). Briefly, emission at 460 nm was measured upon excitation at 355 nm. 455 nm was taken as a cutoff value.

Determining Cell Death, MMP, (Mito)ROS, and Polyamine Uptake via Flow Cytometry. When measuring cell death, cells were collected, briefly centrifuged (450 × *g*, 5 min), resuspended in fluorescence-activated cell sorting (FACS) buffer (PBS without Ca^{2+} and Mg^{2+}, supplemented with 1% wt/vol bovine serum albumin) (3854.3, Roth) and subsequently incubated with 2 μg/mL propidium iodide or 5 nM SYTOX Red (10 min, 4 °C) before quantifying the mean fluorescent intensity with either the Attune Cytometer (Life Technologies) for one-dye experiments or the Canto II AIG equipped with BD FacsDIVA software version 6 (BD Biosciences) for simultaneous detection of two dyes.

When analyzing MMP, ROS, MitoROS, or BODIPY-labeled polyamine uptake, cells were treated with 0.1 μM tetramethylrhodamine methyl ester (35 min, 37 °C), 10 μM DCFDA (35 min, 37 °C) (CM-H2DCFDA, Thermo Fisher Scientific), 3 μM MitoSOX (35 min, 37 °C) (M36008, Thermo Fisher Scientific), or 5 μM BODIPY-labeled polyamine (2 h, 37 °C), respectively. Next, cells were immediately collected and further processed for flow cytometry analysis as described above, with (Fig. S6) or without the SYTOX Red incubation step.

Metabolomics. Metabolomics was performed as previously described (9, 72).

***C. elegans* Strains and Culture.** All strains were cultured on nematode growth medium (NGM) plates with *Escherichia coli* strain OP50 as food source (73) and maintained at 20 °C. Strains were obtained from the *Caenorhabditis* Genetics Center (CGC), University of Minnesota, Minneapolis, MN. The following strains were used in this study: Bristol N2 as the wild-type (control) strain, *catp-6(ok3473)* IV, SJ4058 (*zcls9*[$P_{hsp\text{-}60}$*GFP*] V), *Ex*[$P_{catp\text{-}6}$*catp-6*::*mKate2*; *rol-6(d)*] (*catp-6(ok3473)* + WT), and *Ex*[$P_{catp\text{-}6}$*catp-6(D465N)*::*mKate2*; *rol-6(d)*] (*catp-6(ok3473)* + D465N). *catp-7(0) catp-6(0); catp-5(0)* animals were obtained as F1 segregants from *catp-7(dx189) catp-6(ok3473)/DnT1* IV, *catp-5(tm4481)* X hermaphrodites.

RNA Interference (RNAi). RNA interference (RNAi) was carried out using *atfs-1(RNAi)* from the Ahringer Library (74) and *mock(RNAi)* as a control (which contains HT115 RNAi bacteria transformed with the empty RNAi vector pPD129.36). The feeding method was performed as previously described (75).

***C. elegans* Lethality Assay.** Rotenone and MitoTEMPO were added to a final concentration of 1.5 μM and 10 mM, respectively, in NGM agar plates. Staged nematodes were placed on control or treatment plates and counted after 60 or 72 h exposure. Missing worms were counted as dead worms.

Analysis of MMP and MitoROS in *C. elegans*. When analyzing MMP or MitoROS, 0.1 μM TMRE or 20 μM MitoSOX was added in NGM plates, respectively. After an incubation at 20 °C overnight in the dark, animals at larval stage 3 were mounted on 2% agarose pads for differential interference contrast and epifluorescence microscopy (Zeiss Axioskop 2 and MetaMorph software) (Molecular Devices Inc.). Whole worms were immobilized with 10 mM levamisole and/or 1 mM sodium azide. Image processing was performed in Fiji/ImageJ 2.0.0; brightness and contrast was adjusted in Fiji/ImageJ 2.0.0. For quantification of the MitoSOX measurements, images were first segmented using MitoSegNet (https://github.com/mitosegnet) (76). Next, Fiji/ImageJ was used as well to measure fluorescence intensity using a binary mask of the raw images to define the regions in which intensity was analyzed.

Statistics. Statistical analysis was performed by using GraphPad Prism 8.1.1. Normality was tested using the Shapiro–Wilk test. Next, ANOVA or Kruskal–Wallis tests were used for multiple comparison with the subsequent Tukey/Dunnett or Dunn post hoc tests, respectively. If only two groups were compared, the Mann–Whitney test or unpaired two-tailed *t* test was applied. Each experiment was repeated at least three times.

Data Availability. All study data are included in the article and supporting information.

ACKNOWLEDGMENTS. This work was funded by the Flanders Research Foundation (FWO) (G094219N to P.V., G092714 and G080517N to V.B., SBO Neuro-TRAFFIC S006617N to V.B. and P.V.; and 1503117N to S.M.), the KU Leuven (LysoCaN C16/15/073 to P.V. and P.A.; OT/14/120 to V.B.), the Queen Elisabeth Foundation for Neurosciences (P.V. and V.B.) and the M. J. Fox Foundation/Aligning Science Across Parkinson's (ASAP-0458; P.V. and V.B.). S.V. and S.v.V. are aspirant FWO research fellows (1S88419N and 11Y7518N). Funding for E.L. and J.Z. was provided by Deutsche Forschungsgemeinschaft (DFG) grant LA3380/2-1. Funding for L.B.-C. was provided by the German Academic Exchange Service (DAAD) (57145465). L.B.-C. and J.Z. were supported by Graduate School Life Science Munich. Some nematode strains were provided by the CGC, which is funded by NIH Office of Research Infrastructure Programs (P40 OD010440). Images were recorded on a Zeiss LSM 780–SP Mai Tai HP DS (Cell and Tissue Imaging Cluster), supported by Hercules AKUL/11/37 and FWO G.0929.15 to Pieter Vanden Berghe, University of Leuven. The DFMO used in this study was a kind gift of Dr. P. M. Woster (Medical University of South Carolina, Charleston, SC). We thank M. Schuermans, A. Florizoone, and M. Crabbe for technical assistance; the Leuven Viral Vector Core for the production of viral vectors; and Dr. Steven Verhelst for the production of fluorescent BODIPY polyamines. We also acknowledge our frequent use of the facilities and equipment of the Cell and Tissue Imaging Cluster (P. Vanden Berghe, KU Leuven), the Metabolomics Core (B. Ghesquière, KU Leuven/Vlaams Instituut voor Biotechnologie), and the FACS Core (P. Andrée Penttila, KU Leuven).

1. A. Ramirez *et al*., Hereditary parkinsonism with dementia is caused by mutations in ATP13A2, encoding a lysosomal type 5 P-type ATPase. *Nat. Genet.* **38**, 1184–1191 (2006).
2. A. Di Fonzo *et al*.; Italian Parkinson Genetics Network, ATP13A2 missense mutations in juvenile parkinsonism and young onset Parkinson disease. *Neurology* **68**, 1557–1562 (2007).
3. C. H. Lin *et al*., Novel ATP13A2 variant associated with Parkinson disease in Taiwan and Singapore. *Neurology* **71**, 1727–1732 (2008).
4. A. Estrada-Cuzcano *et al*., Loss-of-function mutations in the ATP13A2/PARK9 gene cause complicated hereditary spastic paraplegia (SPG78). *Brain* **140**, 287–305 (2017).

5. J. Bras, A. Verloes, S. A. Schneider, S. E. Mole, R. J. Guerreiro, Mutation of the parkinsonism gene ATP13A2 causes neuronal ceroid-lipofuscinosis. *Hum. Mol. Genet.* **21**, 2646–2650 (2012).
6. R. Spataro *et al*., Mutations in ATP13A2 (PARK9) are associated with an amyotrophic lateral sclerosis-like phenotype, implicating this locus in further phenotypic expansion. *Hum. Genomics* **13**, 19 (2019).
7. M. Audano, A. Schneider, N. Mitro, Mitochondria, lysosomes, and dysfunction: Their meaning in neurodegeneration. *J. Neurochem.* **147**, 291–309 (2018).
8. B. Dehay *et al*., Loss of P-type ATPase ATP13A2/PARK9 function induces general lysosomal deficiency and leads to Parkinson disease neurodegeneration. *Proc. Natl. Acad. Sci. U.S.A.* **109**, 9611–9616 (2012).
9. S. van Veen *et al*., ATP13A2 deficiency disrupts lysosomal polyamine export. *Nature* **578**, 419–424 (2020).
10. C. F. Bento, A. Ashkenazi, M. Jimenez-Sanchez, D. C. Rubinsztein, The Parkinson's disease-associated genes ATP13A2 and SYT11 regulate autophagy via a common pathway. *Nat. Commun.* **7**, 11803 (2016).
11. A. M. Gusdon, J. Zhu, B. Van Houten, C. T. Chu, ATP13A2 regulates mitochondrial bioenergetics through macroautophagy. *Neurobiol. Dis.* **45**, 962–972 (2012).
12. A. Grunewald *et al*., ATP13A2 mutations impair mitochondrial function in fibroblasts from patients with Kufor-Rakeb syndrome. *Neurobiol. Aging* **33**, 1843.e1–1843.e7 (2012).
13. N. Minois, D. Carmona-Gutierrez, F. Madeo, Polyamines in aging and disease. *Aging (Albany NY)* **3**, 716–732 (2011).
14. A. E. Pegg, Functions of polyamines in mammals. *J. Biol. Chem.* **291**, 14904–14912 (2016).
15. A. E. Pegg, The function of spermine. *IUBMB Life* **66**, 8–18 (2014).
16. T. Holemans *et al*., A lipid switch unlocks Parkinson's disease-associated ATP13A2. *Proc. Natl. Acad. Sci. U.S.A.* **112**, 9040–9045 (2015).
17. C. M. Tanner *et al*., Rotenone, paraquat, and Parkinson's disease. *Environ. Health Perspect.* **119**, 866–872 (2011).
18. H. C. Ha *et al*., The natural polyamine spermine functions directly as a free radical scavenger. *Proc. Natl. Acad. Sci. U.S.A.* **95**, 11140–11145 (1998).
19. X. Wu *et al*., New insights into the role of spermine in enhancing the antioxidant capacity of rat spleen and liver under oxidative stress. *Anim. Nutr.* **3**, 85–90 (2017).
20. H. Shoji *et al*., Effects of human milk and spermine on hydrogen peroxide-induced oxidative damage in IEC-6 cells. *J. Pediatr. Gastroenterol. Nutr.* **41**, 460–465 (2005).
21. J. E. Rider *et al*., Spermine and spermidine mediate protection against oxidative damage caused by hydrogen peroxide. *Amino Acids* **33**, 231–240 (2007).
22. J. B.-F. N. Toro-Funes, M. T. Veciana-Nogués, M. Izquierdo-Pulido, M. C. Vidal-Carou, In vitro antioxidant activity of dietary polyamines. *Food Res. Int.* **51**, 141–147 (2013).
23. E. Løvaas, G. Carlin, Spermine: An anti-oxidant and anti-inflammatory agent. *Free Radic. Biol. Med.* **11**, 455–461 (1991).
24. S. Martin *et al*., Protection against mitochondrial and metal toxicity depends on functional lipid binding sites in ATP13A2. *Parkinsons Dis.* **2016**, 9531917 (2016).
25. J. Lotharius, K. L. O'Malley, The parkinsonism-inducing drug 1-methyl-4-phenylpyridinium triggers intracellular dopamine oxidation. A novel mechanism of toxicity. *J. Biol. Chem.* **275**, 38581–38588 (2000).
26. N. Simola, M. Morelli, A. R. Carta, The 6-hydroxydopamine model of Parkinson's disease. *Neurotox. Res.* **11**, 151–167 (2007).
27. D. Crosiers *et al*., Juvenile dystonia-parkinsonism and dementia caused by a novel ATP13A2 frameshift mutation. *Parkinsonism Relat. Disord.* **17**, 135–138 (2011).
28. N. Li *et al*., Mitochondrial complex I inhibitor rotenone induces apoptosis through enhancing mitochondrial reactive oxygen species production. *J. Biol. Chem.* **278**, 8516–8525 (2003).
29. E. Eruslanov, S. Kusmartsev, Identification of ROS using oxidized DCFDA and flow-cytometry. *Methods Mol. Biol.* **594**, 57–72 (2010).
30. M. E. Kauffman *et al*., MitoSOX-based flow cytometry for detecting mitochondrial ROS. *React. Oxyg. Species (Apex)* **2**, 361–370 (2016).
31. S. Kasai *et al*., Role of the ISR-ATF4 pathway and its cross talk with Nrf2 in mitochondrial quality control. *J. Clin. Biochem. Nutr.* **64**, 1–12 (2019).
32. M. W. Pellegrino, A. M. Nargund, C. M. Haynes, Signaling the mitochondrial unfolded protein response. *Biochim. Biophys. Acta* **1833**, 410–416 (2013).
33. S. Demirsoy *et al*., ATP13A2/PARK9 regulates endo-/lysosomal cargo sorting and proteostasis through a novel PI(3, 5)P2-mediated scaffolding function. *Hum. Mol. Genet.* **26**, 1656–1669 (2017).
34. R. Vanhoutte, J. P. Kahler, S. Martin, S. van Veen, S. H. L. Verhelst, Clickable polyamine derivatives as chemical probes for the polyamine transport system. *ChemBioChem* **19**, 907–911 (2018).
35. D. H. Yan *et al*., Different intracellular polyamine concentrations underlie the difference in the inward rectifier K(+) currents in atria and ventricles of the guinea-pig heart. *J. Physiol.* **563**, 713–724 (2005).
36. M. Bourdenx *et al*., Nanoparticles restore lysosomal acidification defects: Implications for Parkinson and other lysosomal-related diseases. *Autophagy* **12**, 472–483 (2016).
37. G. Landau *et al*., Expression profiling and biochemical analysis suggest stress response as a potential mechanism inhibiting proliferation of polyamine-depleted cells. *J. Biol. Chem.* **287**, 35825–35837 (2012).
38. E. J. Lambie, P. J. Tieu, N. Lebedeva, D. L. Church, B. Conradt, CATP-6, a *C. elegans* ortholog of ATP13A2 PARK9, positively regulates GEM-1, an SLC16A transporter. *PLoS One* **8**, e77202 (2013).
39. J. Zielich *et al*., Overlapping expression patterns and functions of three paralogous P5B ATPases in *Caenorhabditis elegans*. *PLoS One* **13**, e0194451 (2018).
40. T. Yoneda *et al*., Compartment-specific perturbation of protein handling activates genes encoding mitochondrial chaperones. *J. Cell Sci.* **117**, 4055–4066 (2004).
41. W. Poewe *et al*., Parkinson disease. *Nat. Rev. Dis. Primers* **3**, 17013 (2017).
42. L. Dalla Via, V. Di Noto, A. Toninello, Binding of spermidine and putrescine to energized liver mitochondria. *Arch. Biochem. Biophys.* **365**, 231–238 (1999).
43. A. Toninello, L. Dalla Via, D. Siliprandi, K. D. Garlid, Evidence that spermine, spermidine, and putrescine are transported electrophoretically in mitochondria by a specific polyamine uniporter. *J. Biol. Chem.* **267**, 18393–18397 (1992).
44. K. Hoshino *et al*., Polyamine transport by mammalian cells and mitochondria: Role of antizyme and glycosaminoglycans. *J. Biol. Chem.* **280**, 42801–42808 (2005).
45. R. Zhang, X. N. Ma, K. Liu, L. Zhang, M. Yao, Exogenous spermine preserves mitochondrial bioenergetics via regulating Src kinase signaling in the spinal cord. *Mol. Med. Rep.* **16**, 3619–3626 (2017).
46. A. N. Clarkson *et al*., Neuroprotective effects of spermine following hypoxic-ischemic-induced brain damage: A mechanistic study. *FASEB J.* **18**, 1114–1116 (2004).
47. M. Yoshino, Y. Yamada, K. Murakami, Activation by spermine of citrate synthase from porcine heart. *Biochim. Biophys. Acta* **1073**, 200–202 (1991).
48. E. Pezzato, V. Battaglia, A. M. Brunati, E. Agostinelli, A. Toninello, Ca2+ -independent effects of spermine on pyruvate dehydrogenase complex activity in energized rat liver mitochondria incubated in the absence of exogenous Ca2+ and Mg2+. *Amino Acids* **36**, 449–456 (2009).
49. I. G. Sava, V. Battaglia, C. A. Rossi, M. Salvi, A. Toninello, Free radical scavenging action of the natural polyamine spermine in rat liver mitochondria. *Free Radic. Biol. Med.* **41**, 1272–1281 (2006).
50. A. Chatr-Aryamontri *et al*., The BioGRID interaction database: 2017 update. *Nucleic Acids Res.* **45**, D369–D379 (2017).
51. A. Heinick *et al*., *Caenorhabditis elegans* P5B-type ATPase CATP-5 operates in polyamine transport and is crucial for norspermidine-mediated suppression of RNA interference. *FASEB J.* **24**, 206–217 (2010).
52. N. Chai *et al*., Spermidine prevents heart injury in neonatal rats exposed to intrauterine hypoxia by inhibiting oxidative stress and mitochondrial fragmentation. *Oxid. Med. Cell. Longev.* **2019**, 5406468 (2019).
53. S. Rajagopalan, A. Rane, S. J. Chinta, J. K. Andersen, Regulation of ATP13A2 via PHD2-HIF1α signaling is critical for cellular iron homeostasis: Implications for Parkinson's disease. *J. Neurosci.* **36**, 1086–1095 (2016).
54. Q. Xu *et al*., Hypoxia regulation of ATP13A2 (PARK9) gene transcription. *J. Neurochem.* **122**, 251–259 (2012).
55. Fde. T. Pinto, G. R. Corradi, D. P. Hera, H. P. Adamo, CHO cells expressing the human P_5-ATPase ATP13A2 are more sensitive to the toxic effects of herbicide paraquat. *Neurochem. Int.* **60**, 243–248 (2012).
56. Z. Liu, T. Zhou, A. C. Ziegler, P. Dimitrion, L. Zuo, Oxidative stress in neurodegenerative diseases: From molecular mechanisms to clinical applications. *Oxid. Med. Cell. Longev.* **2017**, 2525967 (2017).
57. J. Blesa, I. Trigo-Damas, A. Quiroga-Varela, V. R. Jackson-Lewis, Oxidative stress and Parkinson's disease. *Front. Neuroanat.* **9**, 91 (2015).
58. A. D. Gitler *et al*., Alpha-synuclein is part of a diverse and highly conserved interaction network that includes PARK9 and manganese toxicity. *Nat. Genet.* **41**, 308–315 (2009).
59. T. Tsunemi, K. Hamada, D. Krainc, ATP13A2/PARK9 regulates secretion of exosomes and α-synuclein. *J. Neurosci.* **34**, 15281–15287 (2014).
60. S. Büttner *et al*., Spermidine protects against α-synuclein neurotoxicity. *Cell Cycle* **13**, 3903–3908 (2014).
61. M. Farina, D. S. Avila, J. B. da Rocha, M. Aschner, Metals, oxidative stress and neurodegeneration: A focus on iron, manganese and mercury. *Neurochem. Int.* **62**, 575–594 (2013).
62. S. M. Kong *et al*., Parkinson's disease-linked human PARK9/ATP13A2 maintains zinc homeostasis and promotes α-Synuclein externalization via exosomes. *Hum. Mol. Genet.* **23**, 2816–2833 (2014).
63. J. S. Park, B. Koentjoro, D. Veivers, A. Mackay-Sim, C. M. Sue, Parkinson's disease-associated human ATP13A2 (PARK9) deficiency causes zinc dyshomeostasis and mitochondrial dysfunction. *Hum. Mol. Genet.* **23**, 2802–2815 (2014).
64. P. M. Quirós *et al*., Multi-omics analysis identifies ATF4 as a key regulator of the mitochondrial stress response in mammals. *J. Cell Biol.* **216**, 2027–2045 (2017).
65. E. Fessler *et al*., A pathway coordinated by DELE1 relays mitochondrial stress to the cytosol. *Nature* **579**, 433–437 (2020).
66. X. Guo *et al*., Mitochondrial stress is relayed to the cytosol by an OMA1-DELE1-HRI pathway. *Nature* **579**, 427–432 (2020).
67. I. M. N. Wortel, L. T. van der Meer, M. S. Kilberg, F. N. van Leeuwen, Surviving stress: Modulation of ATF4-mediated stress responses in normal and malignant cells. *Trends Endocrinol. Metab.* **28**, 794–806 (2017).
68. Z. Galehdar *et al*., Neuronal apoptosis induced by endoplasmic reticulum stress is regulated by ATF4-CHOP-mediated induction of the Bcl-2 homology 3-only member PUMA. *J. Neurosci.* **30**, 16938–16948 (2010).
69. J. C. Gully *et al*., Up-regulation of activating transcription factor 4 induces severe loss of dopamine nigral neurons in a rat model of Parkinson's disease. *Neurosci. Lett.* **627**, 36–41 (2016).
70. X. Sun *et al*., ATF4 protects against neuronal death in cellular Parkinson's disease models by maintaining levels of parkin. *J. Neurosci.* **33**, 2398–2407 (2013).
71. L. Wu *et al*., Salubrinal protects against rotenone-induced SH-SY5Y cell death via ATF4-parkin pathway. *Brain Res.* **1549**, 52–62 (2014).
72. J. A. Byun *et al*., Analysis of polyamines as carbamoyl derivatives in urine and serum by liquid chromatography-tandem mass spectrometry. *Biomed. Chromatogr.* **22**, 73–80 (2008).
73. S. Brenner, The genetics of *Caenorhabditis elegans*. *Genetics* **77**, 71–94 (1974).
74. R. S. Kamath, J. Ahringer, Genome-wide RNAi screening in *Caenorhabditis elegans*. *Methods* **30**, 313–321 (2003).
75. L. Timmons, D. L. Court, A. Fire, Ingestion of bacterially expressed dsRNAs can produce specific and potent genetic interference in *Caenorhabditis elegans*. *Gene* **263**, 103–112 (2001).
76. C. A. Fischer *et al*., MitoSegNet: Easy to use deep learning segmentation for analysing mitochondrial morphology. *iScience* **23**, 101601 (2020).